

Chaotic vibrations of flexible curvilinear beams in temperature and electric fields



J. Awrejcewicz^{a,b,*}, V.A. Krysko^c, I.E. Kutepov^c, N.A. Zagniboroda^c, V. Dobriyan^c, I.V. Papkova^c, A.V. Krysko^d

^a Department of Automation, Biomechanics and Mechatronics, Lodz University of Technology, 1/15 Stefanowski St., 90-924 Lodz, Poland

^b Department of Vehicles, Warsaw University of Technology, 84 Narbutt Str., 02-524 Warsaw, Poland

^c Department of Mathematics and Modeling, Saratov State Technical University, Politehnicheskaya 77, 410054 Saratov, Russian Federation

^d Department Applied Mathematics and Systems Analysis, Saratov State Technical University, Politehnicheskaya 77, 410054 Saratov, Russian Federation

ARTICLE INFO

Article history:

Received 20 March 2014

Received in revised form

4 May 2015

Accepted 4 May 2015

Available online 13 May 2015

Keywords:

Curvilinear Euler–Bernoulli beams

Heat transfer equations

Electric fields

Lyapunov exponents

Chaos

ABSTRACT

In this paper regular and chaotic vibrations of flexible curvilinear beams with (and without) the action of temperature and electric fields are studied. Results obtained are based on the reduction of PDEs governing non-linear dynamics of straight and curvilinear beams to large sets of non-linear ODEs putting emphasis on reliability and validation of the results. In spite of the applied classical approaches to study bifurcational and chaotic dynamics, we have employed 2D and 3D Morlet wavelets and we have computed first four Lyapunov exponents. Numerous results are reported regarding scenarios of the transition from regular to chaotic vibrations including the occurrence of hyper-hyper chaos and deep chaos. Snap-through phenomena have been detected and analyzed, and the influence of boundary conditions of three types of the considered fields (mechanical, thermal and electrical) as well as of temperature on non-linear dynamics of the beam have been reported.

© 2015 Elsevier Ltd. All rights reserved.

1. Introduction

There are numerous papers/monographs devoted to the study of dynamics of beams embedded either into an electric field or thermal field separately, and only a few papers address a simultaneous action of both fields on non-linear dynamics of beams.

The influence of electric field on free transverse vibrations of smart beams was studied by Krommer and Irschik [1].

Static and dynamic instabilities of the MEMs cantilever beam system subjected to weak and strong disturbances were investigated by Liu et al. [2]. They illustrated and analyzed period doubling, chaos and strange attractors for both open- and closed-loop cantilever systems subjected to strong disturbances.

Closed-form solutions of Euler–Bernoulli beams with singularities (flexural stiffness and slope discontinuities) are proposed in reference [3]. The continuity conditions are set into the flexural stiffness model and are included in the proposed procedure.

Zamianian and Khaden [4] studied microbeam dynamics under an electric actuation assuming that the microbeam midplane is

stretched when it is deflected. Altering DC electric actuation in a microswitch system exhibits a saddle-node bifurcation point. Depending on the system parameters, periodic, quasi-periodic and pull-in instability can be achieved. The beam chaotic behavior is studied using Melnikov's approach.

Towfighian et al. [5] investigated the closed-loop dynamics of a chaotic electrostatic microbeam actuator with two wells of potential and with two distinct chaotic attractors. Period doubling, reverse period doubling, one-well and two-well chaos, as well as superharmonic resonances are reported, among others.

Barari et al. [6] applied variational iteration and parameterized perturbation methods to investigate the non-linear vibration of Euler–Bernoulli beams subjected to axial loads.

Shen et al. [7] analyzed the Euler–Bernoulli beam model where the absorbed heat flux on the beam surface depended on the beam deformation. The coupled thermal-structural analysis allowed them to predict a cantilever beam movement from eclipse with large incident angles of solar radiation.

Li et al. [8] studied non-linear equilibrium equations of the slender pinned-fixed Euler–Bernoulli beams regarding their buckling behavior.

A thin-walled composite beam including the interaction between structural deformations and incident heating was studied by Ko and Kim [9]. The beam model includes transverse shear deformation and rotary inertia, as well as primary and secondary

* Corresponding author.

E-mail addresses: awrejcew@p.lodz.pl (J. Awrejcewicz), tak@san.ru (V.A. Krysko), ilyakutepov@yandex.ru (I.E. Kutepov), tssrat@mail.ru (N.A. Zagniboroda), Dobriy88@yandex.ru (V. Dobriyan), ikrazzova@mail.ru (I.V. Papkova), anton.krysko@gmail.com (A.V. Krysko).

warping effects. Steady-state thermal response was examined using the uncoupled analysis, whereas thermal flutter was studied by the coupled thermal-structural method.

Li et al. [10] analyzed the fundamental frequency of slender Euler beams embedded into the thermal field under various boundary conditions. The post-buckling behavior of functionally graded material beams with edge crack effects was investigated by Ke et al. [11], Li et al. [12] analyzed thermal stability of nonlinear vibrations of a hybrid functionally graded Timoshenko beam with both clamped edges.

Gilat and Aboudi [13] applied the Lyapunov exponents methodology to study dynamic buckling of composite plates undergoing a sudden thermal or mechanical loading. The approach involving Lyapunov exponents to the quantitative analysis of continuous mechanical systems was applied in both works.

Wu [14] used Hamilton's principle to derive the equations of motion of a pinned beam with transverse magnetic fields and thermal loads. It was shown that the transient vibratory behavior of the beam was influenced by the magnetic and thermal loads; for example, the period of vibration increased with the increase of the magnetic fields and temperatures.

Pull-in instability of the double-clamped microscale beams actuated by a suddenly applied electrostatic force and subjected to non-linear squeeze film damping was investigated by Krylov [15] through monitoring the largest Lyapunov exponent evolution.

Li et al. [16] studied vibrations of functionally graded material beams with surface-bounded piezoelectric layers in thermal environment based on the Euler–Bernoulli beam theory. The beams were covered with piezoelectric layers and subjected to thermo-mechanical loadings. However, the authors reduced the problem to two sets of coupled ordinary differential equations. They showed that the temporal force produced in the piezoelectric layers by the voltage could efficiently increase the critical buckling temperature and the natural frequency.

Non-linear vibrations of the functionally graded material beam bounded with/without piezoelectric layers in a thermal environment were studied by Wang et al. [17] who analyzed pre/post-buckling phases of non-linear vibrations.

Yu et al. [18] studied free vibration of thermal post-buckled functionally graded material beams subjected to both temperature rise and voltage. They showed that three lower frequencies of the pre-buckled (buckled) beam decreased (increased) with the temperature rise, among others.

As it has already been mentioned, there are also works dealing with the problems of non-linear beam dynamics with thermal and electrical excitations. Non-linear vibrations of thermo-electrically post-buckled rectangular functionally graded piezoelectric beams were studied by Komijani et al. [19]. Thermo-electro-mechanical beam properties were graded across the beam thickness, and both in-plane and out-of-plane boundary conditions were considered. The effects of boundary conditions, beam geometry, actuator voltage, and thermal environment action were studied.

The general numerical approach used in this work, as employed to structural members, has already been presented in our earlier papers [21–27]. This type of the studied problem has been analyzed briefly in reference [25]. However, the mentioned short report concerned a straight beam.

Our work is organized in the following way. The flexible curvilinear beam model is introduced in Section 2, where also the types of heat boundary conditions are defined. Then the influence of boundary conditions is briefly illustrated in Section 3. Section 4 deals with the scenarios of transition into chaotic regimes. Chaotic vibrations of the curvilinear beam embedded into a temperature field are studied in Sections 5 and 6 for different types of heat boundary conditions using FFT (Fast Fourier Transform) and LE (Lyapunov Exponent) characteristic of different beam

curvature and temperature magnitude. Section 7 illustrates the effect of beam curvature on the solution of the heat transfer equation, whereas the influence of the electric field on the beam dynamics is illustrated and discussed in Section 8. Concluding remarks are presented in Section 10.

2. Beam model

We consider a one-layer thin flexible curvilinear beam of length l , height h and geometric curvature $k_x = 1/R_x$, where R_x is the curvature radius. The beam is loaded through continuous load along the beam surface $q(x, t)$, acting in the normal direction to the middle beam surface (Fig. 1).

A mathematical model of the beam is based on the hypotheses of shallow shells introduced by Reissner and Vlasov. Namely, for shallow spherical shells the ratio of deflection f to the smallest shell plane dimension of $(f/a) \leq 1/8$ (Reissner) or $(f/a) \leq 1/5$ (Vlasov) and the geometry in space coincides with that of plane.

The mathematical model of the curvilinear beam is governed by a system of non-linear partial differential equations (PDEs) describing the motion of a beam element taking into account energy dissipation which is represented by the occurrence of damping coefficient ε . The non-dimensional form of PDEs regarding displacements is as follows

$$\begin{aligned} \frac{\partial^2 u}{\partial x^2} - k_x \frac{\partial w}{\partial x} + L_3(w, w) - \frac{\partial^2 u}{\partial t^2} &= 0, \\ \frac{1}{\lambda^2} \left\{ -\frac{1}{12} \frac{\partial^4 w}{\partial x^4} + k_x \left[\frac{\partial u}{\partial x} - k_x w - \frac{1}{2} \left(\frac{\partial w}{\partial x} \right)^2 - w \frac{\partial^2 w}{\partial x^2} \right] \right. \\ &+ L_1(u, w) + L_2(w, w) \left. \right\} + q - \frac{\partial^2 w}{\partial t^2} - \varepsilon \frac{\partial w}{\partial t} = 0, \\ L_1(u, w) &= \frac{\partial^2 u}{\partial x^2} \frac{\partial w}{\partial x} + \frac{\partial u}{\partial x} \frac{\partial^2 w}{\partial x^2}; \quad L_2(w, w) = \frac{3}{2} \left(\frac{\partial w}{\partial x} \right)^2 \frac{\partial^2 w}{\partial x^2}; \\ L_3(w, w) &= \frac{\partial w}{\partial x} \frac{\partial^2 w}{\partial x^2}, \end{aligned} \quad (1)$$

where: $L_1(u, w)$, $L_2(w, w)$, $L_3(w, w)$ are the non-linear operators; $w(x, t)$ – normal deflection of the beam element; $u(x, t)$ – longitudinal displacement of the beam element; ε – coefficient of dissipation of the surrounding medium; E – Young modulus; h – height of the beam transversal cross section; γ – specific material gravity; g – Earth acceleration; k_x – geometric beam curvature; t – time; $q = q_0 \sin(\omega_p t)$ – external load; q_0 – amplitude; ω_p – frequency.

Non-dimensional parameters are introduced in the following way:

$$\begin{aligned} \bar{\lambda} &= \frac{a}{h}; \quad \bar{w} = \frac{w}{h}; \quad \bar{u} = \frac{ua}{h^2}; \quad \bar{x} = \frac{x}{a}; \quad \bar{t} = \frac{t}{\tau}; \quad \tau = \frac{a}{p}; \quad p = \sqrt{\frac{Eg}{\gamma}}; \\ \bar{\varepsilon} &= \frac{\varepsilon}{p}; \quad \bar{q} = \frac{qa^4}{h^4 E}; \quad \bar{k}_x = \frac{k_x a}{\lambda}. \end{aligned}$$

Bars over the non-dimensional quantities are omitted in Eq. (1). The following boundary conditions are applied: one beam end is

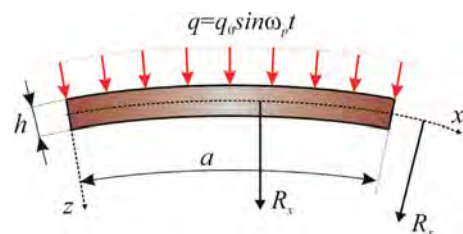


Fig. 1. Flexible curvilinear beam.

Table 1
Types of heat boundary conditions.


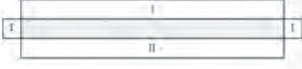

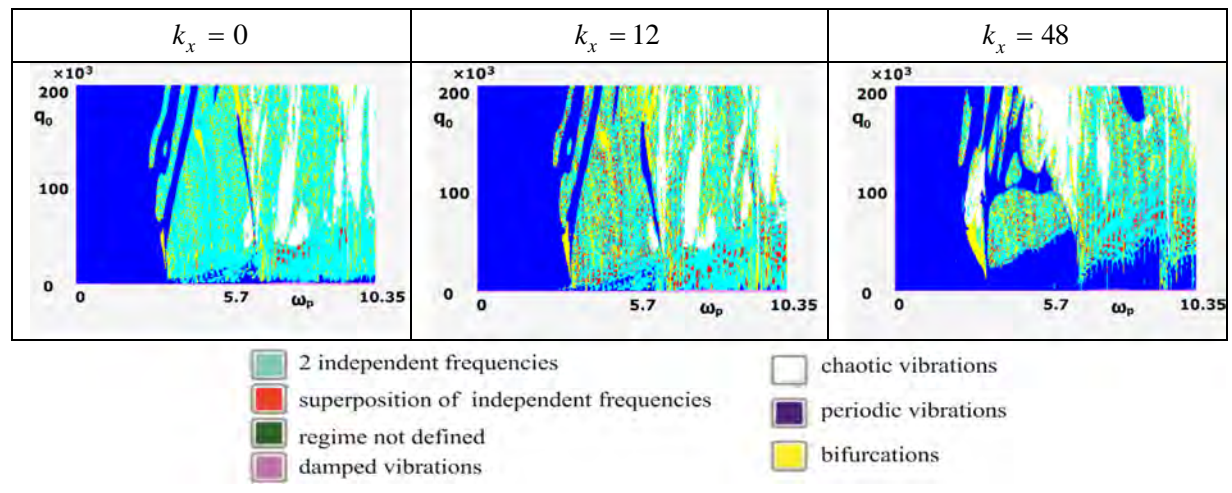
Type 1 (T1)					(4)
$T(x, z) = const$	$z = -1/2$	$0 \leq x \leq 1$	I		
$T(x, z) = 0$	$z = 1/2$	$0 \leq x \leq 1$	I		
$T(x, z) = 0$	$x = 1$	$-1/2 \leq z \leq 1/2$	I		
$T(x, z) = 0$	$x = 0$	$-1/2 \leq z \leq 1/2$	I		
Type 2 (T2)					(5)
$T(x, z) = const$	$z = -1/2$	$0 \leq x \leq 1$	I		
$T(x, z) = \frac{\partial T}{\partial z}$	$z = 1/2$	$0 \leq x \leq 1$	II		
$T(x, z) = 0$	$x = 1$	$-1/2 \leq z \leq 1/2$	I		
$T(x, z) = 0$	$x = 0$	$-1/2 \leq z \leq 1/2$	I		
Type 3 (T3)					(6)
$T(x, z) = const$	$z = -1/2$	$0 \leq x \leq 0,5$	I		
$T(x, z) = \frac{\partial T}{\partial z}$	$z = -1/2$	$0,5 \leq x \leq 1$	II		
$T(x, z) = 0$	$z = 1/2$	$0 \leq x \leq 1$	I		
$T(x, z) = 0$	$x = 1$	$-1/2 \leq z \leq 1/2$	I		
$T(x, z) = 0$	$x = 0$	$-1/2 \leq z \leq 1/2$	I		

Table 2
Vibration charts for different k_x .



simply supported ($x = 0$), whereas the other one is clamped ($x = a$)

$$w(0, t) = w(a, t) = u(0, t) = u(a, t) = w'_{xx}(a, t) = w''_{xx}(0, t) = 0, \quad (2)$$

and the following initial conditions are applied

$$w(x, 0) = \dot{w}(x, 0) = u(x, 0) = \dot{u}(x, 0) = 0. \quad (3)$$

In reference [20], for the curvilinear beams made from isotropic material, the following heat transfer equation $\Delta T + 2k_x(\partial T/\partial z) = 0$ was derived and studied. In what follows we employ the same shallow conditions and we consider also the Laplace type heat transfer equation $\Delta T = 0$ with the boundary conditions given in Table 1:

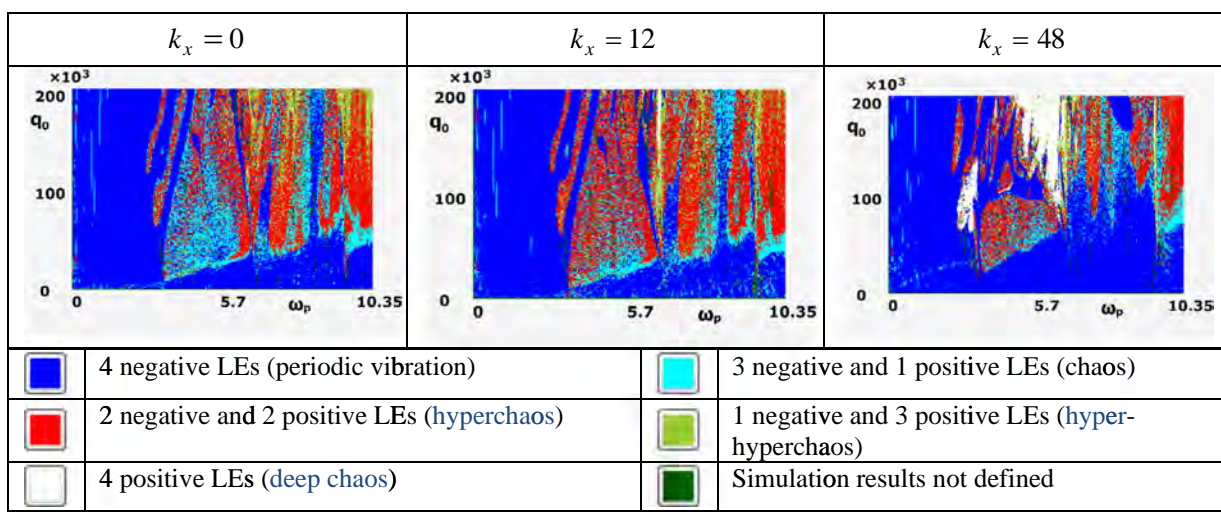
PDEs (1) are reduced to ODEs via Finite Difference Method (FDM) of the second order. The latter procedure allowed us to

obtain the following set of ODEs:

$$\begin{aligned} \ddot{u}_t &= \Lambda_{x^2}(u_i) - k_x \Lambda_x(w_i) + \Lambda_x(w_i) \Lambda_{x^2}(w_i), \\ \ddot{w}_t + \varepsilon \dot{w}_t &= \frac{1}{\lambda^2} \left\{ -\frac{1}{12} \Lambda_{x^4}(w_i) + k_x \left[\Lambda_x(u_i) - k_x \Lambda_x(w_i) - \frac{1}{2} \Lambda_{x^2}(w_i) \right] - \right. \\ &\quad \left. - \Lambda_{x^2}(u_i) \Lambda_x(w_i) + \Lambda_{x^2}(w_i) \Lambda_x(u_i) + \frac{3}{2} (\Lambda_x(w_i))^2 \Lambda_{x^2}(w_i) \right\} + q. \end{aligned} \quad (7)$$

The obtained system of the second-order ODEs (7) with corresponding boundary conditions (yielded by the application of FDM) are then reduced to the first-order ODEs, which are further solved by the fourth-order Runge-Kutta method. In the papers [21–27] we proved that this method was sufficient and efficient. Since the governing equations of the curvilinear beam differ from those of the flexible straight linear beam only due to the terms related to

Table 3
Charts of Lyapunov exponents for different k_x .



the geometric curvatures, we may follow the method for validation of results given in the mentioned references.

First, we study beam vibrations without the action of the temperature field. Applying FDM, unit interval $x \in [0; 1]$ is divided into 120 parts, and the following parameters are fixed during the computation: $\lambda = 100$, $\varepsilon = 1$, $k_x = 0, 12, 48$. Table 2 reports charts showing types of beam vibrations for the set of parameters $\{q_0, \omega_p\}$ including quasi-periodic vibration (2 independent frequencies), damped vibrations, periodic and chaotic vibrations, as well as bifurcation zones. The zones, where the vibrational regime has not been defined, correspond to the lack of convergence of the used numerical integration algorithms.

In other words, in order to identify a point color, i.e. the vibrational regime of an investigated point of the chart, the numerical analysis has been carried out with the help of power spectra analyses through FFT. Irrespective of this type of analysis, we included also the charts of Lyapunov exponents (LE). The latter ones are constructed in the plane of control parameters $\{\omega_p, q_0\}$ in a similar way, i.e. four Lyapunov exponents have been computed at each point of the (q_0, ω) plane.

It is remarkable that an increase of the beam curvature yields a larger area of periodic vibrations (blue color). For instance, there is a peninsula-like zone of periodicity for relatively high values of both ω_p and q_0 . The increase of curvature in the interval $k_x = [0, 12]$ does not yield sufficient changes in the charts of vibration types. All possible non-linear dynamical phenomena are presented (quasi-periodic orbits marked as vibrations with two independent frequencies, high-dimensional tori with vibrations being the superposition of independent frequencies, chaotic vibrations and zones of bifurcations). The main difference in comparison to the case of $k_x = 0$ is that in the case of $k_x = 12$ the existence of quasi-periodic orbits with superposition of independent frequencies is more visible (the number of red drops increased). The case of $k_x = 48$ differs from the previous ones because the area of chaotic zones increased significantly versus the remaining studied cases.

In order to validate the so far presented and discussed charts based on a study of the power frequency spectrum, we have computed in addition four Lyapunov exponents. This approach is not limited only to validate the earlier results, but also it allows us to define the strength of chaotic zones. Namely, we have computed the first four Lyapunov exponents, and hence we can detect chaos, hyperchaos, hyper-hyperchaos, and deep chaos.

Table 3 reports charts regarding the Lyapunov exponents which have been found using the Wolf algorithm (four largest Lyapunov

exponents are computed). Comparison of Tables 3 and 2 shows a remarkable convergence of the various types of analysis carried out. Each type of the chart exhibits its own characteristic aspect, whereas their common analysis allows us to understand the global system behavior. An increase of the beam curvature yields extension of the space with regular dynamics (four exponents are negative), whereas after dynamical stability loss the vibrational process is transited into a deep chaos (four LEs are positive), which cannot be detected either for a straight line beam or for a beam with small curvature.

3. The influence of mechanical boundary conditions

Three types of the beam support with the following fixed parameters ($k_x = 48$, $\lambda = 100$) are studied.

1. Both ends of the beam are fixed:

$$w(0, t) = w(l, t) = u(0, t) = u(l, t) = w'_x(0, t) = w'_x(l, t) = 0. \quad (8)$$

2. Both ends of the beam are pinned:

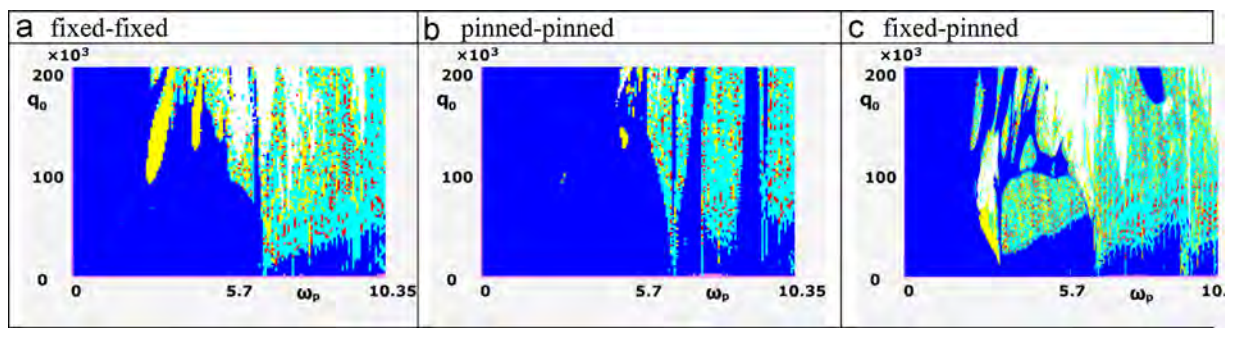
$$w(0, t) = w(l, t) = u(0, t) = u(l, t) = M_x(0, t) = M_x(l, t) = 0. \quad (9)$$

3. One beam end is fixed, whereas the other one is pinned:

$$w(0, t) = w(l, t) = u(0, t) = u(l, t) = w'_x(0, t) = M_x(l, t) = 0. \quad (10)$$

The remaining parameters are the same as those in the previous case. The reported charts (Table 4) of vibration types show that the boundary conditions influence significantly the non-linear beam dynamics. In almost whole chart area of the investigated control parameters the regular dynamics (periodicity and quasi-periodicity) dominates in the case of a pinned-pinned support. In the case of fixed-fixed support the zone of periodic vibrations covers less than half of the chart, and tongues of bifurcation zones (yellow) and chaos (white) are clearly visible for high values of ω_p and q_0 . In the case of mixed boundary conditions, the area of chaos increases significantly, and chaos can be reached even for relatively low values of control parameters. Surprisingly, there is a tongue of the periodic zone for high values of q_0 and ω_p .

Table 4
Vibration charts for different boundary conditions.



Charts presented in Table 4 are constructed with the help of the power spectrum analysis via FFT, and the same color notation as that applied in Table 3 is used.

4. Scenario of transitions into chaos

We study the beam with curvature $k_x = 48$ and the following fixed parameters: $n = 120$, $\lambda = 100$, $\varepsilon = 1$. The analysis was carried out for fixed excitation frequency $\omega_p = 5.7615$ and different values of the excitation amplitude. Tables 5–8 show the following characteristics: (1) Fourier power spectrum ($t \in [1836, 2348]$); $\chi = 0.5$; (2) Poincaré pseudo-map; (3) phase portrait; (4) modal portrait; (5) autocorrelation function; (6) the shape of beam deflection in time instant $t = 1836$; (7) the shape of beam deflection versus time $t \in [1836, 1852]$; (8) 2D Morlet wavelet; (9) 3D Morlet wavelet.

The following conclusions can be formulated on the basis of the results given in Tables 5–8. For the amplitude of excitation $q_0 = 57500$ (Table 5) periodic vibrations are obtained. In the modal portrait we may follow the occurrence of the attractor, but its magnitude is so small that it is not validated either via the phase portrait or the Fourier power spectrum. A slight increase of the excitation amplitude up to $q_0 = 62500$ yields the occurrence of an independent frequency and a set of dependent frequencies appears. Then the phase portraits exhibit an attractor (the modal portrait is collapsed and the Poincaré map shows the attractor). In the interval $q_0 = [64500, 83000]$ results of the simulation are changed qualitatively though small changes in both the Poincaré section and in the energy distribution along the power spectrum are visible (the graphical results are not reported here). For the amplitude $q_0 = 85000$ (Table 6) a collapse of both the Poincaré section and phase portrait is observed and the system transits via a jump (stiff bifurcation) into the periodic state (for $q_0 = 86000$, not reported here). However, this state is not robust and one observes a transition into chaos in the interval $q_0 = [86500, 87000]$ (2D Morlet wavelet exhibits the intermittency of frequencies, whereas 3D Morlet wavelet validates the energy pumping into low frequencies). The Poincaré map splits into the attractor validated also by the phase and modal portraits, and the autocorrelation function strongly decreases in time. Observe that the changes described so far influence strongly both the charts of vibration character and the maximum beam deflection. For $q_0 = 86500$ the deflection is equal to 1.75, for $q_0 = 87000$ it reaches the value of 4.25, and for $q_0 = 87500$ it is equal to 10.5 (the two latter results are not reported here). The maximum deflection moves along the x coordinate to the beam center and the system resists to give a feedback to the non-symmetric boundary conditions. In fact, our thin curvilinear beam exhibits buckling and loses a possibility to react to the external load which is well demonstrated by time evolutions of the beam deflections.

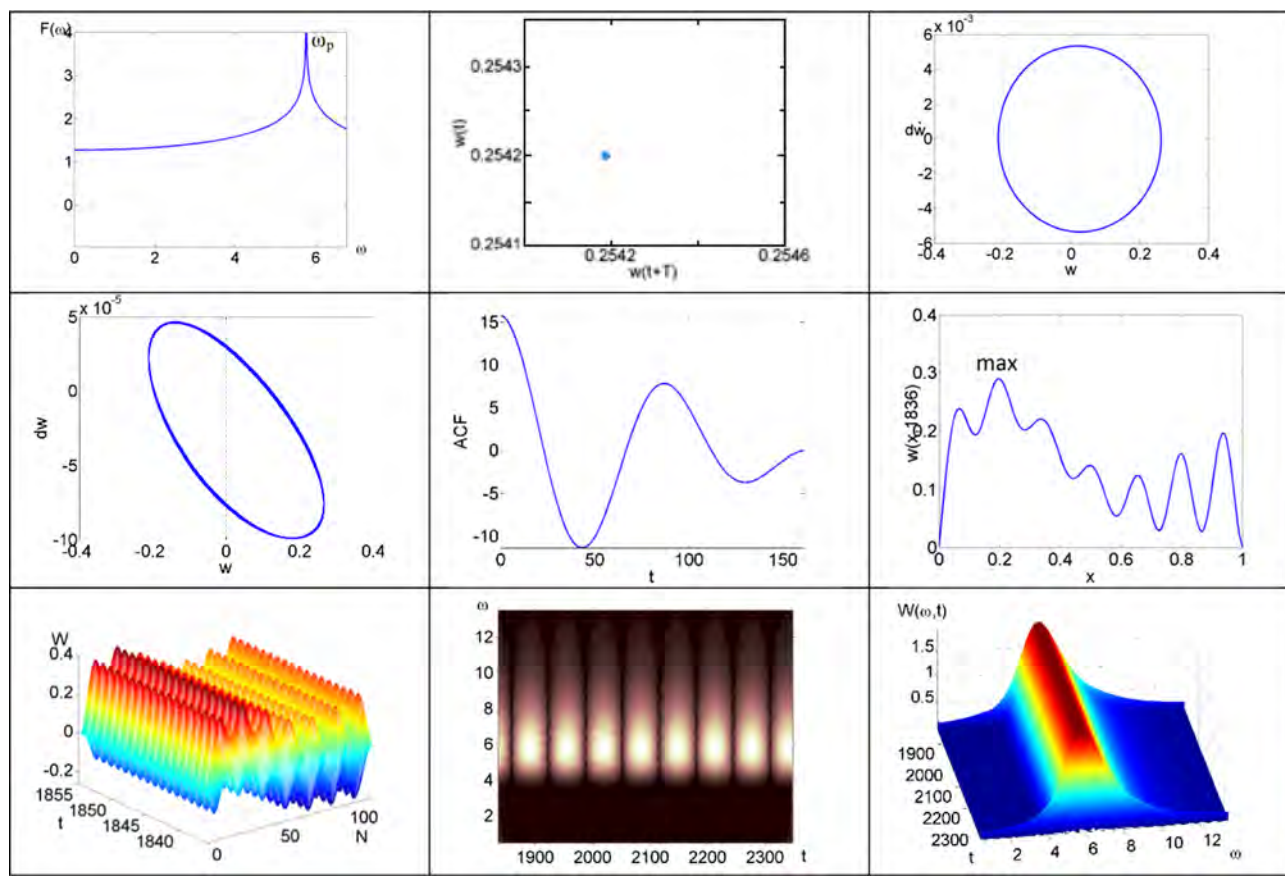
A further analysis has only a theoretical aspect, since the beam deflection is out of the initially introduced mechanical hypotheses. All amplitudes of the external loads applied further deal with the occurrence of the Lorenz attractor on the phase portraits. The autocorrelation function strongly decreases. The Fourier power spectrum becomes noisy, a broad-band frequency basis is observed and a deep chaotic regime is exhibited.

Analysis of the Fourier power spectrum allows us to monitor the following scenarios of transition into chaos. For the amplitude of excitation less than $q_0 = 57,500$ periodic vibrations are observed at frequency $\omega_p = 5.7615$. An increasing excitation amplitude implies the occurrence of frequency $\omega_1 = 2.614$ being non-commensurable with the fundamental ones, and simultaneously the linearly dependent frequency $\omega_2 = \omega_p - \omega_1$ is generated. This process takes place further and the Ruelle–Takens–Newhouse scenario follows. It is basically visible for excitation amplitude $q_0 = 62500$. This scenario is continued up to $q_0 = 86000$, when the system transits again into periodic vibrations. The increase of the excitation amplitude from $q_0 = 86500$ to $q_0 = 87000$ implies the occurrence of intermittency (this is exhibited by the 2D Morlet wavelet) which yields the increase of stochasticity of the spectrum. However, frequencies $\omega_1 = 2.405$, $\omega_2 = \omega_p - \omega_1$ can be distinguished, and the Ruelle–Takens–Newhouse scenario appears. This scenario is conserved until $q_0 = 87500$. A further increase of the excitation amplitude results in a novel dynamical phenomenon, i.e. two scenarios of transition into chaos appear simultaneously. Though for $q_0 = 88500$ (Table 7) one may distinguish fundamental frequencies ω_p , two frequencies ω_1 and $\omega_2 = \omega_p - \omega_1$ remaining from the previous Ruelle–Takens–Newhouse scenario, as well as frequencies $\omega_3 = \omega_p/2 = 2.884$, $\omega_4 = \omega_p/4 = 1.424$, $\omega_5 = 3/4\omega_p = 4.308$ appear. The values of frequencies ω_3 , ω_4 , ω_5 validate the Hopf bifurcation, i.e. the Feigenbaum period doubling scenario is exhibited while transiting into chaos. However, for $q_0 = 95500$ the system dynamics changes, since the birth of frequencies $\omega_1 = \omega_2/2 = 2.884$, as well as $\omega_2 = 1.387$, $\omega_3 = 1.497$, $\omega_4 = 4.271$, $\omega_5 = 4.369$ is observed. It should be emphasized that frequencies ω_2 and ω_3 are located around $\omega_p/4 = 1.436$, whereas frequencies ω_4 and ω_5 around $3/4\omega_p = 4.307$, i.e. both implicit and explicit Hopf bifurcations as well as the damped Ruelle–Takens–Newhouse scenario are exhibited. When carrying out a similar analysis of vibrations of the curvilinear beam in the interval from $q_0 = 95000$ to $q_0 = 96500$ it is clear that a few times the system shows a jump-type reconstruction into two configuration states. A doubled system regime is robust even for higher values of q_0 , unless it transits into the deep chaotic state with fully broadband Fourier spectrum (Table 7).

5. Chaotic vibrations in the temperature field ($k_x = 12$)

Tables 9 and 10 give the analysis of the influence of stationary temperature field for problems of type 1 to 3 (boundary conditions for

Table 5
Beam characteristics ($q_0 = 57500$, $\omega_p = 5.7615$).



temperature fields are defined in Table 1) for the curvilinear beam with curvatures $k_x = 12; 24$. The first reported graph presents the color palette of the temperature field regarding beam thickness and length. Further, relations $w_{\max}(0, 5)(q_0)$ and scales obtained with the help of FFT and Lyapunov exponents (LE) estimations for the temperature field intensity $T=0; 200; 300$ are given. The following non-linear dynamics has been detected: periodic (all LEs are negative), chaotic (one LE is positive), hyperchaotic (two LEs are positive), hyper-hyperchaotic (three LEs are positive) and deep chaotic (four LEs are positive).

Consider the case of heat boundary condition of type 1 (T1) and beam curvature $k_x = 12$ (Table 9). In interval $q_0 = [8, 10]$ temperature $T \in [0, 300]$ does not influence linear dependence $w_{\max}(q_0)$ (the three curves overlap). Another observation is that the reported scales of FFT and LE are in agreement and provide more information by supplementing each other. In the beginning it is also shown that the occurrence of temperature causes beam center deflections of about 1.4 units ($q_0 = 0$). In the case of $T = 0$ the increase of q_0 causes a parabolic increase of w_{\max} up to the value of $w_{\max} = 2$, then the increase is less dynamic and after reaching $q_0 = 6.3$ a snap-through occurs.

The snap-through phenomena exhibited by relation $w_{\max}(q_0)$ are associated with deep chaotic dynamics. A qualitatively similar behavior has been observed in the two remaining heat boundary conditions of type 2 and 3 (not reported here). In both cases only the qualitatively different temperature distribution has been detected (in the case of T3 a break of distribution of the temperature symmetry has been observed).

We carried out a similar computational analysis regarding beam curvature for $k_x = 24$. Here, we report only one example associated with the heat boundary conditions of type 2 (Table 10).

In this case there is a wider interval where two curves of $w_{\max}(q_0)$ are almost linear and overlap each other but only for the cases of $T = 200$ and $T = 300$. In the case of $T = 0$ there are four snap-through phenomena. Furthermore, beginning from $q_0 \in [12, 15]$ the value of w_{\max} is almost constant in the case of $T = 200$ and $T = 300$ (higher values correspond to lower temperature). Again, in the case of boundary condition T3 the lack of symmetric heat distribution over the beam length was observed (not reported here).

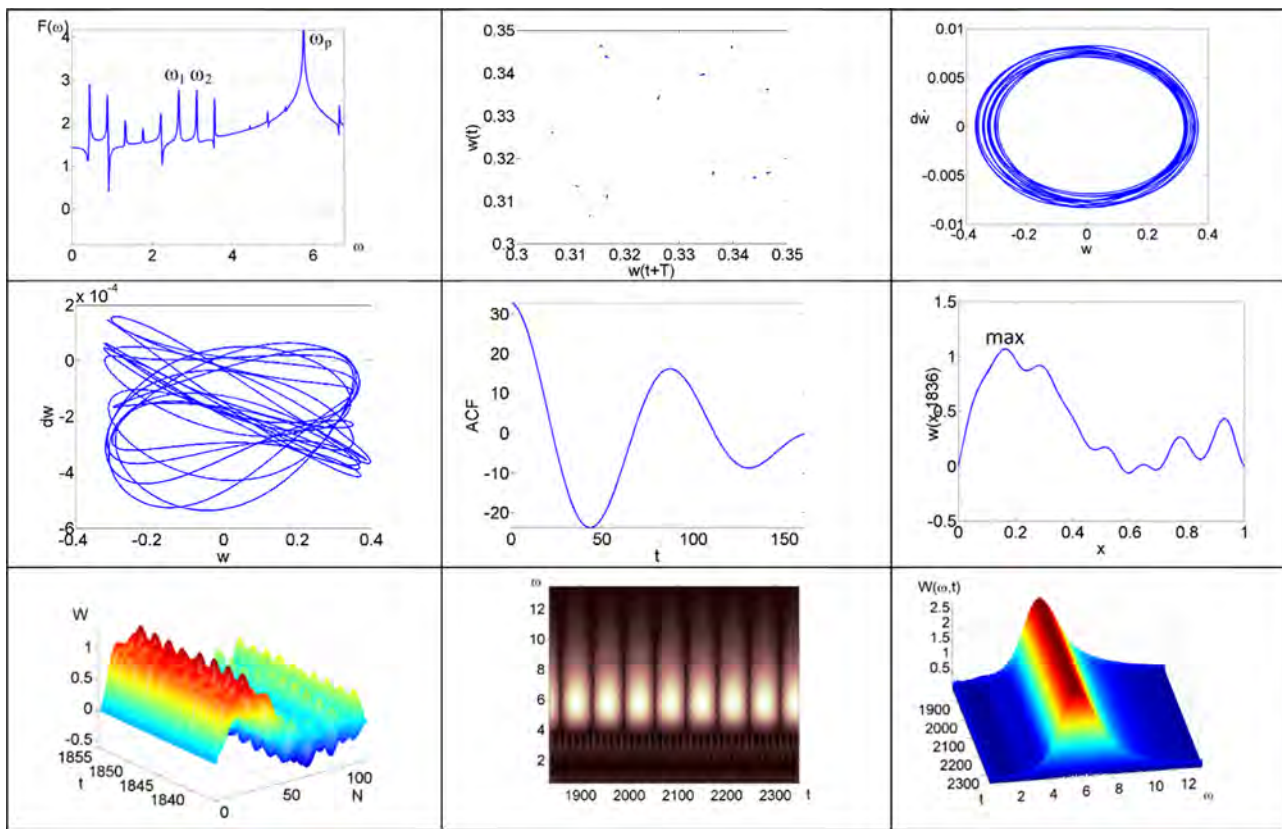
In general, the analysis of results implies that the temperature field increase causes an increase of periodic vibration zones. The zones of different chaos types decrease essentially. Parameter k_x largely affects the curvilinear beam vibrations. An increased temperature field intensity implies vanishing of the deep chaos, and hence an increase in the value of q_0 causes also the death of hyperchaos state.

6. The influence of heat transfer boundary conditions and beam curvature

In this section we briefly address the problem devoted to the impact of three types of heat boundary conditions as well as beam curvature on maximum vibrations monitored in the beam center. Table 11 presents relations $w_{\max}(0.5)(q_0)$ for three types of boundary conditions (Table 1) vs. $k_x = 0; 12; 24$. Initial deflections serve as initial conditions of the Cauchy problem (initial system state is defined via the relaxation method [28,29]).

The first row of Table 11 presents the same temperature value but associated with three different types of the heat boundary conditions. An increase of beam curvature k_x implies the increase

Table 6
Beam characteristics ($q_0 = 85000$, $\omega_p = 5.7615$).



of w_{max} . The deepest snap-through phenomenon occurs for $k_x = 24$, and in the case of type 3 heat boundary conditions. The second row of Table 11 reports the influence of heat boundary conditions for the assumed beam curvature $k_x = 0, 12, 24$. It is noteworthy that in the case of curvature $k_x = 12$ the type of heat boundary conditions introduces almost negligible differences in the $w_{max}(q_0)$ characteristics up to the value of $q_0 = 10$.

7. The influence of k_x on the solution of heat transfer equation

In this section we are going to solve the 3D heat transfer equation in order to define the temperature field for a curvilinear beam. For shells made from an isotropic material a stationary heat transfer equation has the following form [20]

$$\frac{\partial^2 T}{\partial x^2} + \frac{\partial^2 T}{\partial z^2} + 2k_x \frac{\partial T}{\partial x} = -\frac{W_0}{\lambda}, \tag{11}$$

where λ stands for the heat transfer coefficient of the isotropic body. As in the previous examples, we do not take into account the internal heat source ($W_0 = 0$). So, Eq. (11) yields

$$\nabla^2 T + 2k_x \frac{\partial T}{\partial x} = 0.$$

Temperature is yielded by the method of boundary elements (the number of FEM elements and nodes associated with FDM are given in Table 12). Analysis of the obtained results shows that in order to get reliable results it is required to increase the number of partitions while k_x is increased.

Fig. 2 illustrates $w_{max}(0.5)(q_0)$ for the problem of type 1 (Table 1) for two fixed parameters $k_x = 12$ and $k_x = 24$. A dotted

(or solid) curve corresponds to the problem, while in Eq. (11) the beam curvature k_x is not taken (or is taken) into account.

Analysis of the relations yields the following result: the increase of k_x implies essential changes in the characteristic $w_{max}(0.5)(q_0)$.

8. The influence of electric field

In this section a mathematical model of a flexible curvilinear beam in the stationary temperature field and electric field is derived. A polarized electro-conducting layer is situated on the beam surface (Fig. 3).

A beam of length a (along the Ox axis), height h (along the Oz axis), and of unit width is considered. The beam material is described in the frame of the linear theory of piezoelectricity. The supported beam is subjected to the action of transversal load $q(x, t)$. Its surfaces $z = \pm h$ are electrically loaded through the potential difference $V(t)$. Surfaces $x = 0, x = a$ are not covered by electrodes. The beam displacements are as follows:

$$u_z = u - z \frac{\partial w}{\partial x}, \quad w_z = w, \quad -h \leq z \leq h, \tag{12}$$

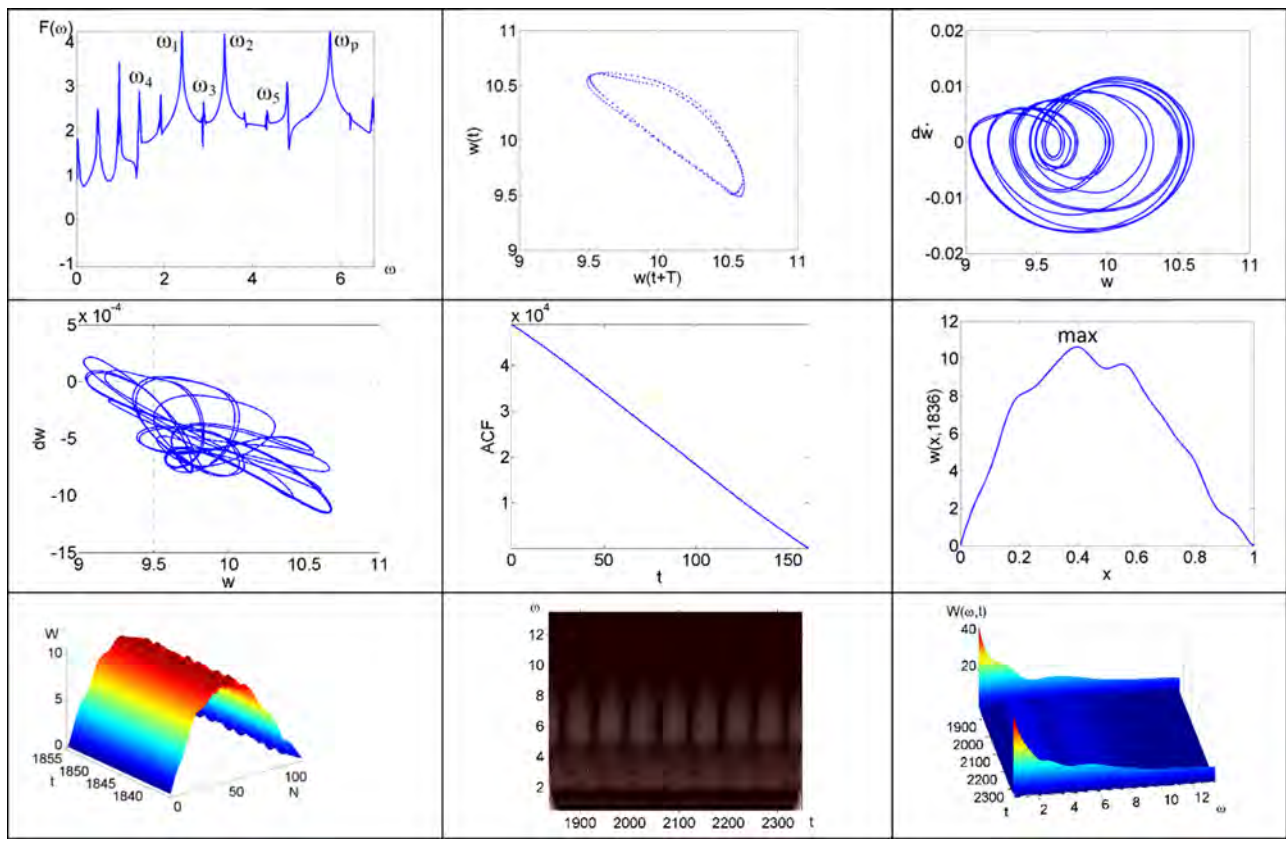
where $u = u(x, t)$ and $w = w(x, t)$ are the beam longitudinal displacement and beam deflection measured regarding the beam middle curve, respectively.

The beam deformation is described by the following formulas

$$\epsilon_{xx} = \frac{\partial u}{\partial x} + \frac{1}{2} \left(\frac{\partial w}{\partial x} \right)^2 - z \frac{\partial^2 w}{\partial x^2}, \quad \epsilon_{zx} = 0. \tag{13}$$

The vector characteristics of the electric field are: $D = D(x, z, t)$ – induction, $E = E(x, z, t)$ – electric field intensity. The state

Table 7
Beam characteristics ($q_0 = 88500$, $\omega_p = 5.7615$).



equations are approximated by the linear direct and inversed piezo-effect and pyro-electric effect, and they have the following form

$$\sigma_{xx} = c_{11}^E (\varepsilon_{xx} - \alpha_T T) - e_{31} E_z,$$

$$D_x = \varepsilon_{11}^S E_x,$$

$$D_z = \varepsilon_{33}^S E_z + e_{31} \varepsilon_{xx} + g_{pyr} T, \quad (14)$$

where: c_{11}^E – elasticity modulus (for the constant electric field), e_{31} – piezoelectric coefficient, $\varepsilon_{11}^S, \varepsilon_{33}^S$ – dielectric permeability (for constant deformation), α_T – coefficient of linear heat extension, $T = \theta(x, z, t) - T_0$ – temperature increase with respect to the temperature T_0 , g_{pyr} – pyro-electric coefficient ($g_{pyr} = (2, \dots, 3) \cdot 10^{-3}$ for direction along the initial polarization and $g_{pyr} = 0$ for the remaining directions). Note, that state Eq. (14) govern the case when the beam material is initially polarized along its thickness. Electrostatic equations have the following form

$$\frac{\partial D_x}{\partial x} + \frac{\partial D_z}{\partial z} = 0, \quad E_x = -\frac{\partial \psi}{\partial x}, \quad E_z = -\frac{\partial \psi}{\partial z}, \quad (15)$$

where $\psi = \psi(x, z, t)$ is the electric potential. The first of Eq. (15), after substituting (13) into (14), takes the following form

$$\frac{e_{31}}{\varepsilon_{33}^S} \frac{\partial^2 w}{\partial x^2} + \frac{\varepsilon_{11}^S}{\varepsilon_{33}^S} \frac{\partial^2 \psi}{\partial x^2} + \frac{\partial^2 \psi}{\partial z^2} - \frac{g_{pyr}}{\varepsilon_{33}^S} \frac{\partial T}{\partial z} = 0. \quad (16)$$

Introducing forces

$$N_x = \int_{-h}^h \sigma_{xx} dz, \quad Q_x = \frac{\partial M_x}{\partial x} = \frac{\partial}{\partial x} \int_{-h}^h \sigma_{xx} z dz,$$

and after a few transformations we get

$$N_x = 2hc_{11}^E \left(\frac{\partial u}{\partial x} + \frac{1}{2} \left(\frac{\partial w}{\partial x} \right)^2 + \frac{e_{31}}{2hc_{11}^E} V(t) - \frac{\alpha_T}{2h} \int_{-h}^h T dz \right),$$

$$Q_x = -\frac{2h^3}{3} c_{11}^E \frac{\partial^3 w}{\partial x^3} - c_{11}^E \alpha_T \int_{-h}^h \frac{\partial T}{\partial x} dz. \quad (17)$$

Projection of the equation governing the motion onto the Ox axis takes the form

$$(2h\rho)(\ddot{u} + \varepsilon_1 \dot{u}) = \frac{\partial N_x}{\partial x}, \quad (18)$$

and after taking into account (17) we get

$$\frac{\partial^2 u}{\partial x^2} + L_3(w, w) - \frac{\alpha_T}{2h} \int_{-h}^h \frac{\partial T}{\partial x} dz = \frac{\rho}{c_{11}^E} (\ddot{u} + \varepsilon_1 \dot{u}). \quad (19)$$

On the other hand, projection of the motion into the Oz axis is

$$\frac{\partial Q_x}{\partial x} + N_x \frac{\partial^2 w}{\partial x^2} + \frac{\partial N_x}{\partial x} \frac{\partial w}{\partial x} + q = (2h\rho)(\ddot{w} + \varepsilon_2 \dot{w}), \quad (20)$$

which, after taking (15) into account, takes the final form

$$L_1(u, w) + L_2(w, w) - \frac{h^2}{3} \frac{\partial^4 w}{\partial x^4} + \frac{q}{2hc_{11}^E} + \left(\frac{e_{31}}{2hc_{11}^E} \right) V(t) \frac{\partial^2 w}{\partial x^2} -$$

$$- \frac{\alpha_T}{2h} \left(\int_{-h}^h \frac{\partial^2 T}{\partial x^2} z dz + \frac{\partial^2 w}{\partial x^2} \cdot \int_{-h}^h T dz + \frac{\partial w}{\partial x} \cdot \int_{-h}^h \frac{\partial T}{\partial x} dz \right) = \left(\frac{\rho}{c_{11}^E} \right) (\ddot{w} + \varepsilon_2 \dot{w}). \quad (21)$$

Eqs. (16), (17) and (21) have the dimensional form. Below, symbol \sim is associated with dimensional quantities, whereas the lack of this symbols denotes non-dimensional quantities. We use

Table 8

Beam characteristics ($q_0 = 96500$, $\omega_p = 5.7615$).

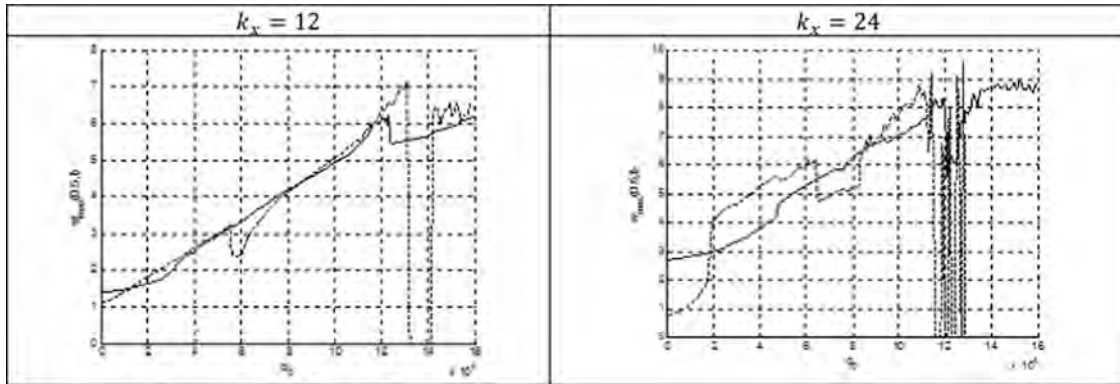
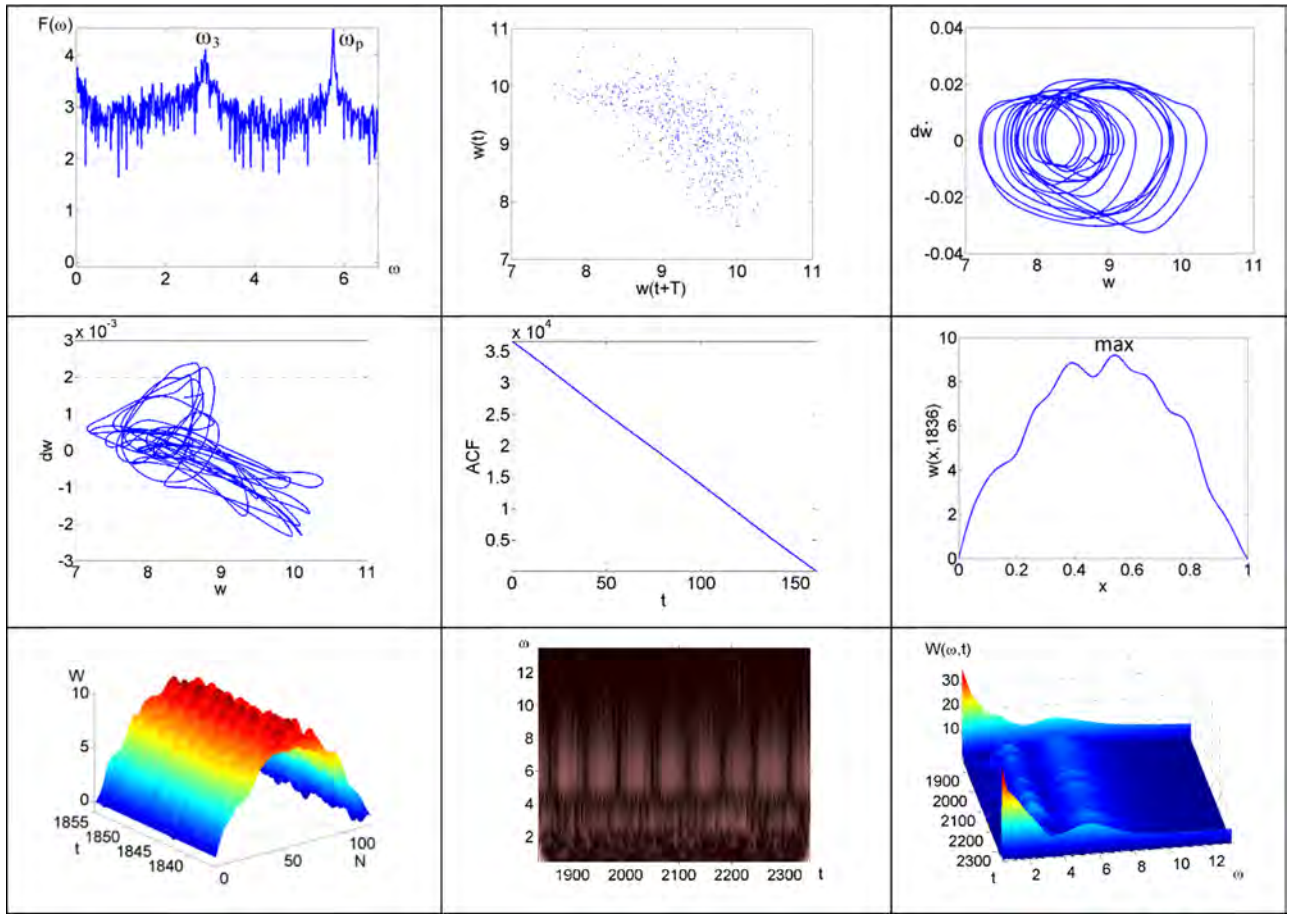


Fig. 2. Beam deflection vs. q_0 for two curvatures.

$$\begin{aligned}
 c &= \sqrt{c_{11}^E/\rho} - \text{velocity}, \quad d_{31} - \text{piezo-modulus}, \\
 \tilde{x} &= ax, \quad \tilde{z} = 2hz, \quad \tilde{u} = \frac{(2h)^2}{a}u, \quad \tilde{w} = 2hw, \quad \lambda = \frac{a}{2h}, \quad \tilde{t} = \frac{a}{c}t, \\
 \tilde{\epsilon}_{1,2} &= \frac{c}{a}\epsilon_{1,2}, \quad \tilde{q} = c_{11}^E \left(\frac{2h}{a}\right)^4 q, \quad \tilde{V} = \frac{1}{\lambda^2} \left(\frac{2h}{d_{31}}\right)V, \quad \tilde{\psi} = \frac{1}{\lambda^2} \left(\frac{2h}{d_{31}}\right)\psi, \quad \tilde{T} = T_0T.
 \end{aligned}
 \tag{22}$$

Eqs. (16), (17) and (21) take the following counter-part form

$$k_1^2 \frac{\partial^2 w}{\partial x^2} + \frac{1}{\lambda^2} \frac{\epsilon_{11}^S}{\epsilon_{33}^S} \frac{\partial^2 \psi}{\partial x^2} + \frac{\partial^2 \psi}{\partial z^2} - k_{pyr}^2 \lambda^2 \frac{\partial T}{\partial z} = 0,$$

$$\begin{aligned}
 \frac{\partial^2 u}{\partial x^2} + L_3(w, w) - \lambda^2 \cdot (\alpha_T T_0) \int_{-1/2}^{1/2} \frac{\partial T}{\partial x} dz &= \ddot{u} + \epsilon_1 \dot{u}, \\
 \frac{1}{\lambda^2} \left(L_1(u, w) + L_2(w, w) - \frac{1}{12} \frac{\partial^4 w}{\partial x^4} + q + k_2^2 \cdot V(t) \cdot \frac{\partial^2 w}{\partial x^2} \right) \\
 - (\alpha_T T_0) \left(\int_{-1/2}^{1/2} \frac{\partial^2 T}{\partial x^2} dz + \frac{\partial^2 w}{\partial x^2} \cdot \int_{-1/2}^{1/2} T dz + \frac{\partial w}{\partial x} \cdot \int_{-1/2}^{1/2} \frac{\partial T}{\partial x} dz \right) &= \ddot{w} + \epsilon_2 \dot{w}.
 \end{aligned}
 \tag{23}$$

In Eq. (23) $k_1^2 = e_{31}d_{31}/\epsilon_{33}^S$ and $k_2^2 = e_{31}/(c_{11}^E d_{31})$ denote the non-dimensional coefficients of the electro-mechanical coupling and

$k_{pyr}^2 = g_{pyr} T_0 d_{31} / \epsilon_{33}^S$ is the non-dimensional coefficient of the pyro-electric coupling.

Furthermore, we have

$$L_1(u, w) = \frac{\partial u}{\partial x} \frac{\partial^2 w}{\partial x^2} + \frac{\partial^2 u}{\partial x^2} \frac{\partial w}{\partial x}, \quad L_2(w, w) = \frac{3}{2} \frac{\partial^2 w}{\partial x^2} \left(\frac{\partial w}{\partial x} \right)^2,$$

$$L_3(w, w) = \frac{\partial w}{\partial x} \frac{\partial^2 w}{\partial x^2} = \frac{1}{2} L_1(w, w). \quad (24)$$

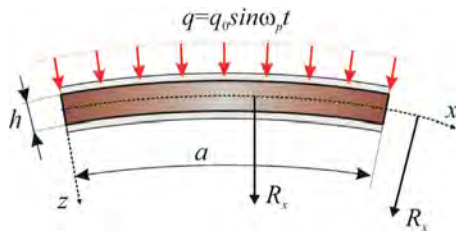


Fig. 3. Flexible curvilinear beam with the electric layer.

9. Initial and boundary conditions for electric potential

For $\psi = \psi(x, z, t)$ the non-dimensional boundary conditions are: $\psi(x, -1/2, t) = -V(t)/2, \psi(x, 1/2, t) = V(t)/2$ ($0 \leq x \leq 1, t > 0$) $\partial\psi/\partial x = 0$ for $x=0, x=1$ ($-1/2 \leq z \leq 1/2, t > 0$). Initial conditions regarding the non-dimensional quantities are as follows:

$$\psi = 0, \quad \frac{\partial\psi}{\partial t} = 0 \quad \text{for } t = 0 \quad (0 \leq x \leq 1, \quad -1/2 \leq z \leq 1/2).$$

Parameters are the same as these adopted previously. Data reported in Table 13 show that for the uncoupled problem (without the influence of the electric field on temperature field), the electric field has only a negligible effect on the chaotic beam dynamics.

10. Concluding remarks

In this final section we shortly summarize the applied methodology and the obtained results putting emphasis on their novelty. First, the object of our study represents a continuous structural member, and hence its dynamics is governed by non-linear PDEs. Furthermore, we study a problem, when our beam is

Table 9
Temperature field scale, $w_{\max}(q_0)$ and FFT/LE (T1, $k_x=12$).

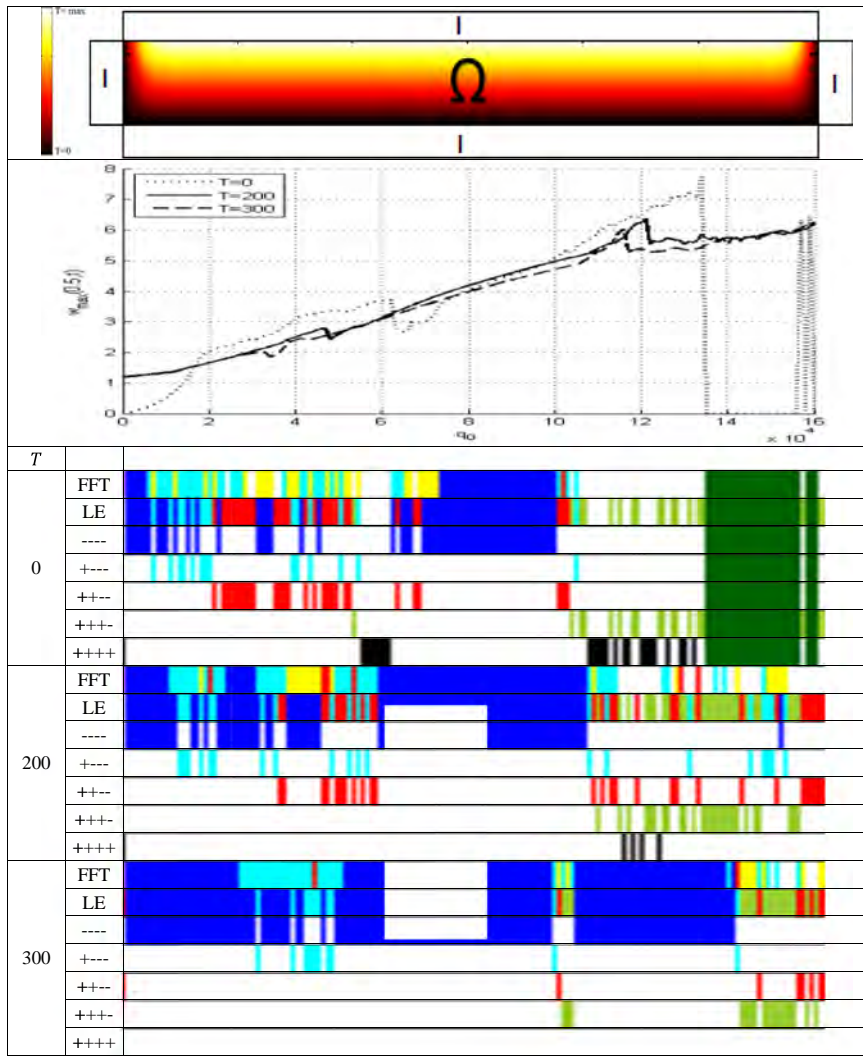
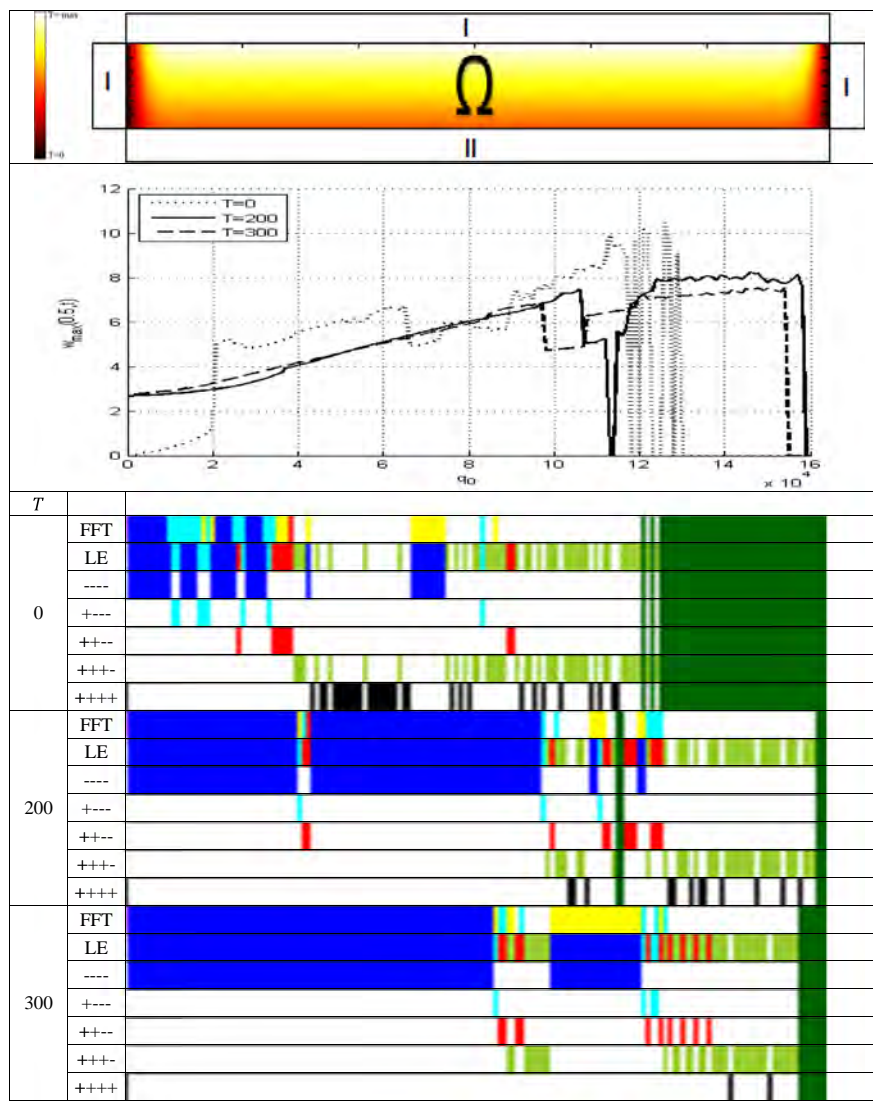


Table 10
Temperature field scale, $w_{\max}(q_0)$ and FFT/LE ($T2, k_x=24$).



located in either thermal environment or is affected by both thermal and electric fields. Each of the PDEs associated either with the action of the mechanical field (the Euler–Bernoulli beam theory with inclusion of the von Kármán non-linearity) or the thermal/electric fields requires different boundary conditions.

The research takes into account strong non-linear dynamic effects, and in particular bifurcational and chaotic vibrations exhibited by the beam. The constructed charts of beam vibration type which are associated with long computational time (each point of the chart requires computation of a set of many nonlinear ODEs with the help of numerous characteristics applied to identify a type of nonlinear dynamics) play a key role in direct engineering applications. It is well known that bifurcational and chaotic dynamics is much more dangerous than the regular one due to the occurrence of large vibration amplitudes. Therefore, the obtained charts may serve as a recipe to make a proper choice of control parameters in order to avoid dangerous dynamical regimes.

It should be emphasized that dynamics of any structural member (beam, plate, shell) governed by non-linear PDEs yields a qualitatively different problem than that originated from dynamical behavior of lumped mechanical systems with either one or a few degrees of freedom. It is clear and well documented in the

existing literature that in many cases we cannot reduce the problem of infinite dimension to that of one- or two-degrees-of-freedom mechanical systems. The usually introduced strong truncation of an infinite set of ODEs may generate erroneous results. This is why the numerical study requires validation and confirmation of reliability of the results. Our research satisfies the mentioned requirements. Furthermore, we proposed a deeper analysis beyond the classical ones, which allows us to offer significant new physical insights in the presented non-linear phenomena using an example of the curvature beam dynamics.

The obtained results are briefly summarized as follows:

- (i) A different form of the PDEs and the associated boundary conditions have been derived;
- (ii) Charts of vibration types (Table 2) and charts of first four Lyapunov exponents (Table 3) for different beam curvatures ($k_x = 0, 12, 48$) have been constructed;
- (iii) The influence of three types of the mechanical boundary conditions on the beam dynamics has been reported in the form of vibration charts (Table 4);
- (iv) Scenarios of transition from regular to chaotic beam vibrations using FFT, Poincaré pseudo-maps, phase portraits,

Table 11
Beam deflection $w_{\max}(0.5)(q_0)$ for different heat boundary conditions type and curvature magnitudes.

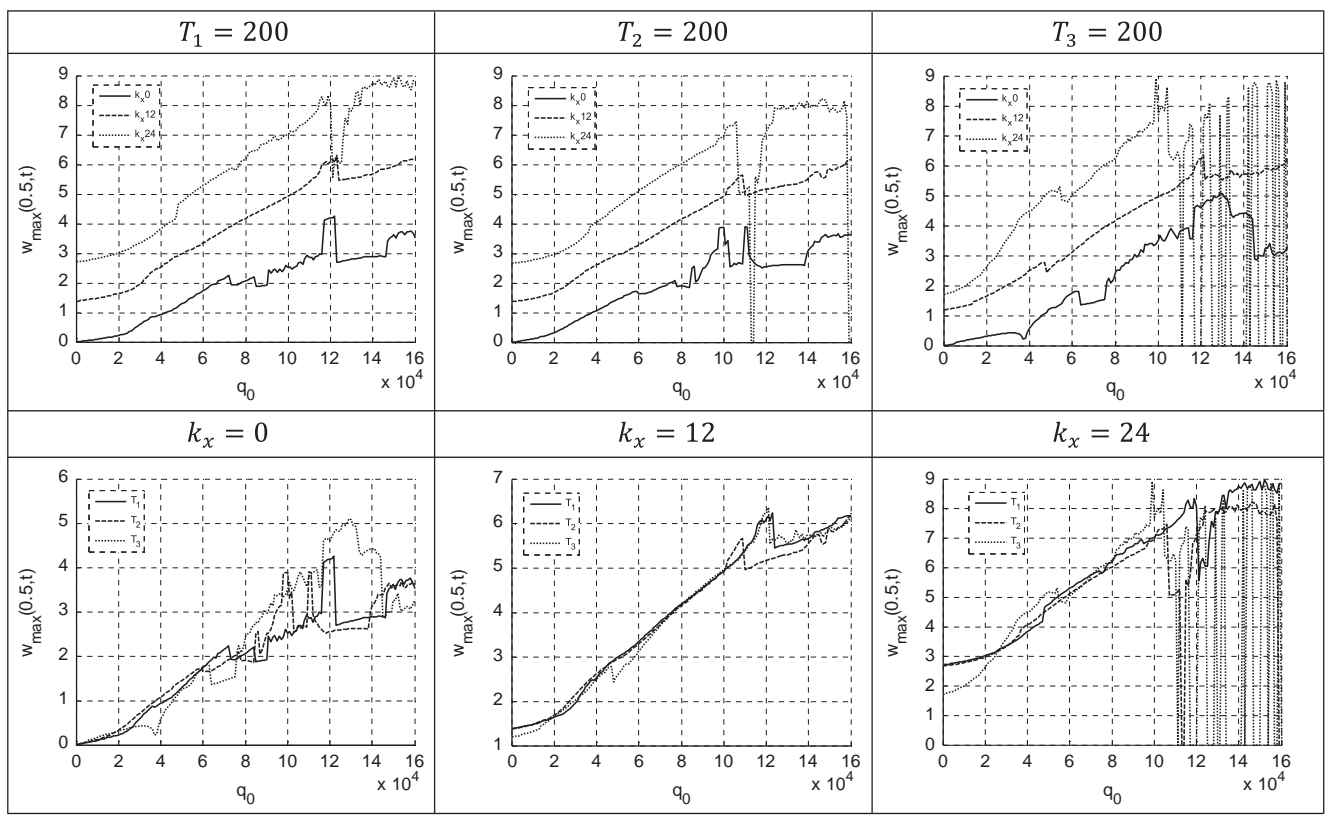
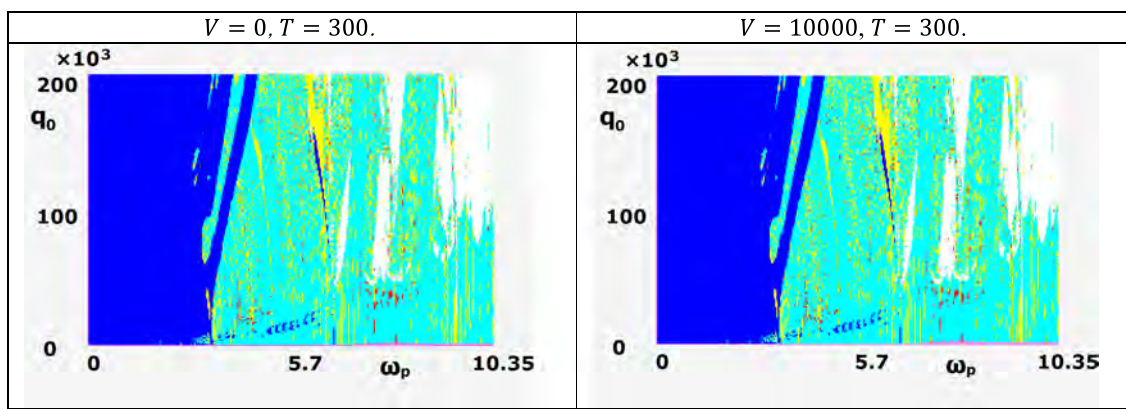


Table 12
Numbers of FEM elements and numbers of nodes (FDM).

Number of elements	$k_x = 12$	$k_x = 24$	Finite differences $m \times n$	$k_x = 12$	$k_x = 24$
32	0.28	0.35	32×32	0.32	0.36
64	0.28	0.35	64×64	0.28	0.31
128	0.28	0.35	128×128	0.28	0.31

Table 13
Vibration chart showing the influence of V .



modal portraits, autocorrelation functions, shapes of beam deflection, 2D and 3D Morlet wavelets have been detected and discussed;

(v) Chaotic vibrations of the beam in the stationary temperature field environment have been studied putting emphasis on the snap-through phenomena exhibited by the $w_{\max}(q_0)$ curves

- with respect to three different types of heat boundary conditions;
- (vi) The effect of beam curvature (in the equation governing heat transfer) on the beam dynamics has been investigated (usually this question is omitted in the existing literature while studying similar types of problems);
- (vii) We have shown that in the case of non-coupling between electric and temperature fields, the electric field action has a negligible impact on non-linear beam dynamics.

Acknowledgments

This paper was financially supported by the National Science Centre of Poland under the grant MAESTRO 2, No. 2012/04/A/ST8/00738, for the years 2013–2016.

References

- [1] M. Krommer, H. Irschik, On the influence of the electric field on free transverse vibrations of smart beams, *Smart Mater. Struct.* 8 (3) (1999), doi:10.1088/0964-1726/8/3/311.
- [2] S. Liu, A. Davidson, Q. Lin, Simulation studies on nonlinear dynamics and chaos in a MEMS cantilever control system, *J. Micromech. Microeng.* 14 (7) (2004) 1064–1073.
- [3] B. Biondi, S. Caddemi, Closed form solutions of Euler–Bernoulli beams with singularities, *Int. J. Solids Struct.* 42 (9–10) (2005) 3027–3044.
- [4] M. Zamanian, S.E. Khadem, Stability analysis of an electrically actuated microbeam using the Melnikov theorem and Poincaré mapping, *Proc. Inst. Mech. Eng. Part C: J. Mech. Eng. Sci.* 225 (2) (2011) 488–497.
- [5] S. Towfighian, G.R. Heppler, E.M. Abdel-Rahman, Analysis of a chaotic electrostatic microoscillator, *J. Comput. Nonlinear Dyn.* 6 (1) (2011) 011001.
- [6] A. Barari, H.D. Kaliji, M. Ghadim, G. Domairry, Non-linear vibration of Euler–Bernoulli beams, *Latin Am. J. Solids Struct.* 8 (2) (2011), <http://dx.doi.org/10.1590/S1679-78252011000200002>.
- [7] Zhenxing Shen, Qiang Tian, Xiaoning Liu, Gengkai Hu, Thermally induced vibrations of flexible beams using Absolute Nodal Coordinate Formulation, *Aerosp. Sci. Technol.* 29 (1) (2013) 386–393.
- [8] S.R. Li, Y.H. Zhou, X. Zheng, Thermal post-buckling of a heated elastic rod with pinned-fixed ends, *J. Therm. Stresses* 25 (1) (2002) 45–56.
- [9] Kyung-Eun Ko, Ji-Hwan Kim, Thermally induced vibrations of spinning thin-walled composite beam, *AIAA J.* 4 (2) (2003) 296–303.
- [10] S.R. Li, Z.C. Teng, Y.H. Zhou, Free vibration of heated, Euler–Bernoulli beams with thermal post-buckling deformations, *J. Therm. Stress.* 27 (9) (2004) 843–856.
- [11] L.L. Ke, J. Yang, S. Kitipornchai, Postbuckling analysis of edge cracked functionally graded Timoshenko beams under end shortening, *Compos. Struct.* 90 (2) (2009) 152–160.
- [12] S.R. Li, H.D. Su, C.J. Cheng, Free vibration of functionally graded material beams with surface-bonded piezoelectric layers in thermal environment, *Appl. Math. Mech.* 30 (8) (2009) 969–982.
- [13] R. Gilat, J. Aboudi, The Lyapunov exponent as a quantitative criterion for the dynamic buckling of composite plates, *Int. J. Solids Struct.* 39 (2002) 467–481.
- [14] Guan-Yuan Wu, Transient vibration analysis of a pinned beam with transverse magnetic fields and thermal loads, *J. Vib. Acoust.* 127 (3) (2005) 247–253.
- [15] S. Krylov, Lyapunov exponents as a criterion for the dynamic pull-in instability of electrostatically actuated microstructures, *Int. J. Non-Linear Mech.* 42 (2007) 626–642.
- [16] Shi-rong Li, Hou-de Su, Chang-jun Cheng, Free vibration of functionally graded material beams with surface-bonded piezoelectric layers in thermal environment, *Appl. Mech. Mater.* 30 (8) (2009) 969–982.
- [17] Y. Fu, J. Wang, Y. Mao, Nonlinear analysis of buckling, free vibration and dynamic stability for the piezoelectric functionally graded beams in thermal environment, *Appl. Math. Model.* 36 (9) (2012) 4323–4340.
- [18] Shu Reng Yu, Hell Su, Jian Ling Fan, Free vibration of functionally graded material beams in a uniform electric field, *Appl. Mech. Mater.* 157–158 (2012) 3–6.
- [19] M. Komijani, Y. Kiani, S.E. Esfahani, M.R. Eslami, Vibration of thermo-electrically post-buckled rectangular functionally graded piezoelectric beams, *Compos. Struct.* 98 (2013) 143–152.
- [20] Ya.S. Podstrigatch, D.N. Shvets, *Thermo-Elasticity of Thin Shells*, Naukova Dumka, Kiev, 1978.
- [21] J. Awrejcewicz, A.V. Krysko, V. Soldatov, V.A. Krysko, Analysis of the nonlinear dynamics of the Timoshenko flexible beams using wavelets, *J. Comput. Nonlinear Dyn.* 7 (1) (2012) 011005-1–011005-14.
- [22] J. Awrejcewicz, V.A. Krysko, I.V. Papkova, A.V. Krysko, Routes to chaos in continuous mechanical systems. Part 1: Mathematical models and solution methods, *Chaos Solitons Fractals* 45 (2012) 687–708.
- [23] J. Awrejcewicz, V.A. Krysko, I.V. Papkova, A.V. Krysko, Routes to chaos in continuous mechanical systems. Part 2: Modelling transitions from regular to chaotic dynamics, *Chaos Solitons Fractals* 45 (2012) 709–720.
- [24] J. Awrejcewicz, V.A. Krysko, I.V. Papkova, A.V. Krysko, Routes to chaos in continuous mechanical systems. Part 3: The Lyapunov exponents, hyper, hyper-hyper and spatial-temporal chaos, *Chaos Solitons Fractals* 45 (2012) 721–736.
- [25] V.A. Krysko, J. Awrejcewicz, I.E. Kutepov, N.A. Zagniboroda, I.V. Papkova, A. V. Serebryakov, A.V. Krysko, Chaotic dynamics of flexible beams with piezoelectric and temperature phenomena, *Phys. Lett. A* 377 (2013) 2058–2061.
- [26] A.V. Krysko, J. Awrejcewicz, I.E. Kutepov, N.A. Zagniboroda, V. Dobriyan, V. A. Krysko, Chaotic dynamics of flexible Euler–Bernoulli beams, *Chaos* 34 (4) (2014) 043130-1–043130-25.
- [27] A.V. Krysko, J. Awrejcewicz, O.A. Saltykova, M.V. Zhigalov, V.A. Krysko, Investigations of chaotic dynamics of multi-layer beams using taking into account rotational inertial effects, *Commun. Nonlinear Sci. Numer. Simul.* 19 (8) (2014) 2568–2589.
- [28] V.I. Fedos'ev, On a certain method of solution to the nonlinear problem of stability of deformable systems, *Appl. Math. Mech.* 27 (1963) 265–274.
- [29] J. Awrejcewicz, V.A. Krysko, *Nonclassical Thermoelastic Problems in Nonlinear Dynamics of Shells*, Springer-Verlag, Berlin Heidelberg, 2003.